Microporous and Mesoporous Materials 264 (2018) 55–59

Contents lists available at ScienceDirect

Microporous and Mesoporous Materials

journal homepage: www.elsevier.com/locate/micromeso

Probing locations of organic structure-directing agents (OSDAs) and host-guest interactions in **CHA**-type SAPO-34/44

Nana Yan[a,b], Hongyi Xu[c], Wenna Zhang[a,b], Tantan Sun[a,b], Peng Guo[a,*], Peng Tian[a,**], Zhongmin Liu[a,***]

[a] National Engineering Laboratory for Methanol to Olefins, Dalian National Laboratory for Clean Energy, Dalian Institute of Chemical Physics, Chinese Academy of Sciences, Dalian, 116023, PR China
[b] University of Chinese Academy of Sciences, Beijing, 100049, PR China
[c] Inorganic and Structural Chemistry, Department of Materials and Environmental Chemistry, Stockholm University, SE-106 91, Stockholm, Sweden

ARTICLE INFO

Keywords:
Rietveld refinement
Simulated annealing
SAPO-34
Different OSDAs
Host-guest interaction

ABSTRACT

In this work, we have synthesized four SAPO-34/44 (framework type code: **CHA**) samples by utilizing different organic structure-directing agent (OSDA) such as cyclohexylamine (CA), n-butylamine (BA), diisopropylamine (DIPA), and dipropylamine (DPA). An approach combining Rietveld refinement and simulated annealing has been successfully applied to determine the location of the individual OSDA and the host (inorganic framework)-guest (OSDA) interaction. The final Rietveld refinements show that 1) one *cha* cage can be occupied by either two OSDAs (CA and BA) in the up-and-down arrangement or one OSDA (DIPA and DPA) in the longitudinal configuration and 2) the classical hydrogen bond between CA/BA and the inorganic framework in SAPO-44-CA and SAPO-34-BA could be identified. The host-guest interactions among these four samples are also investigated by FT-IR, which are consistent with Rietveld refinement results. The approach employed here could be applicable for the host-guest investigation in other crystalline porous materials.

1. Introduction

Aluminophosphate (ALPO) molecular sieves with neutral frameworks were first reported by Union Carbide in 1982 [1]. The AlO_4 and PO_4 tetrahedra distribute alternatingly, generating a three-dimensional (3D) framework with well-defined cavities or channels of molecular sizes. The substitutions of silicon, metal, or both of them into the ALPO frameworks provide the possibilities of creating a series of novel microporous materials SAPO [2], MeAPO [3], or MeAPSO [3,4], respectively. This chemical replacement also enriches the structural diversity of ALPO-based molecular sieves. Among these materials, SAPO molecular sieves have been intensively investigated in both industry and academic communities due to their high thermal stability, moderate acidities and tailored crystallographic structure. SAPO molecular sieves with the **CHA** framework type code (FTC) such as SAPO-34 and SAPO-44 have attracted increasing attention since they have displayed a high selectivity of ethylene and propylene in the methanol-to-olefin (MTO) reaction [5,6], a promising catalytic performance in the selective reduction of NO_x [7,8], and a high CO_2/CH_4 selectivity [9,10].

The organic structure-directing agent (OSDA) has played an indispensable role in the synthesis of SAPO molecular sieves. It is interesting to note that a variety of OSDAs could be utilized to synthesize **CHA**-type SAPO molecular sieves [11–20]. Knowing the locations of OSDAs and exploring the interactions between the framework (host) and OSDAs (guest) will shed light on the phenomenon “one specific structure/multiple OSDAs” [21] and even provide an alternative perspective in understanding the catalytic performance [22–24]. There are a number of approaches to locate the OSDAs in the framework, such as molecular modeling [25–27], spectroscopic characterization [11,28], and refinement against X-ray diffraction data [20,29–32]. The first one, in most cases, lacks the experimental data to support the built models while the second one is challenging to provide atomic coordinates of guest species. Refinement against single crystal X-ray diffraction (SCXRD) data is a conventional way to locate the guest species and identify the host-guest interaction. For example, Bennett et al. have identified the locations of cyclohexylamines in CoAPO-44 and CoAPSO-44 (FTC: **CHA**) through refinement against SCXRD data and revealed that the two cyclohexylamines on the ***ab***-plane are arranged in an up-and-down configuration within one *cha* cage [31]. Pastore et al. have synthesized **CHA**-type SAPO form CAL-1 using two different OSDAs (n-

* Corresponding author.
** Corresponding author.
*** Corresponding author.
E-mail addresses: pguo@dicp.ac.cn (P. Guo), tianpeng@dicp.ac.cn (P. Tian), zml@dicp.ac.cn (Z. Liu).

https://doi.org/10.1016/j.micromeso.2018.01.002
Received 31 October 2017; Received in revised form 28 December 2017; Accepted 1 January 2018
Available online 02 January 2018
1387-1811/

butylamine and hexamethyleneimine) [29]. They also investigated the host-guest interaction by combining SCXRD refinement and Fourier Transform infrared spectroscopy (FT-IR).

The above investigations about the host-guest interactions are mainly based on the refinement against SCXRD data, which requires the crystals to be sufficiently large in size. Unfortunately, sometimes SAPO molecule sieves are prone to crystallize in sub-micrometer in size, which is too small to be studied by conventional SCXRD technique. Thus, powder X-ray diffraction (PXRD) technique becomes an alternative approach. Turrina et al. have located the positions of OSDAs in SAPO molecular sieves including SAPO-56 (FTC: **AFX**), STA-18 (**SFW**), and STA-19 (**GME**) based on the Rietveld refinement against PXRD [33]. The combined results of molecular modeling and Rietveld refinement against PXRD indicate that some SAPOs could be synthesized in a targeted way.

In this article, four as-made SAPO-34/44 samples synthesized by cyclohexylamine (CA), n-butylamine (BA), diisopropylamine (DIPA), and dipropylamine (DPA) were studied. By successfully locating the OSDAs in the *cha* cage using a combination of simulated annealing and Rietveld refinement against PXRD data, we intend to take a further step to understand the interactions between guest molecules and inorganic framework in SAPO-34/44.

2. Experimental

2.1. Synthesis

SAPO-34/44 was synthesized using the conventional hydrothermal method. The gel was prepared by the following procedure. The mixture of aluminum source (pseudo-boehmite (67.5 wt%) or aluminum isopropoxide), water, phosphoric acid (85 wt%), silicon resource (TEOS or fumed silica), and OSDAs was stirred at room temperature to form a homogenous gel. Then the gel was transferred to a stainless steel autoclave and crystallized at 200 °C for 24 h under the rotation condition of 70 r/min. After the crystallization, the solid products were obtained by centrifugation, washed with distilled water three times, and dried in air at 120 °C overnight. The proton form samples were obtained by calcined at 873 K for 4 h.

2.2. Characterization

The PXRD data used for phase identification was collected on a PANalytical X'Pert PRO X-ray diffractometer with CuKα radiation (λ = 1.5418 Å). The elemental compositions (Si, Al, and P) of the samples were determined by a Philips Magix-601 X-ray fluorescence spectroscopy (XRF). Thermogravimetry analysis (TGA) was carried out on a TA Q-600 analyzer with a heating rate of 10 °C/min under an air flow of 100 mL/min. The morphology and size of the crystals were determined by scanning electron microscope (SEM) on a Hitachi SU8020 microscope. The FT-IR spectra were recorded on a Bruker Tensor-27 IR spectrometer in the frequency range 4000–400 cm^{-1} with a resolution of 4 cm^{-1}. Four as-made SAPO samples were measured in the scattered reflection mode and FT-IR spectra were obtained after the sample was dehydrated at 200 °C for an hour and cooled to 20 °C under an air flow of 30 mL/min. The proton form samples were measured under identical conditions as the as-made samples, except they were cooled to 100 °C. In addition, four liquid samples of OSDA were measured in the transmission mode. Raman spectra were measured on JY Company spectrograph with spectral resolution of 4 cm^{-1}. The laser line at 244 nm was used as an exciting source. The power of laser line, measured at the samples, was about 0.2 mW. The spectra of all samples were recorded at room temperature. The solid-state NMR experiments were recorded on a Bruker Avance III 600 spectrometer equipped with a 14.1 T wide-bore magnet using a 4 mm WVT double resonances MAS probe. The resonance frequencies of ^{1}H and ^{13}C are 600.13 and 150.9 MHz respectively. ^{13}C MAS NMR spectra were recorded using cross polarization (CP, $^{1}H \rightarrow {}^{13}C$) sequence with a contact time of 4 ms and a recycle delay of 2 s at the spinning rate of 12 kHz. 400 scans were accumulated to achieve a satisfactory signal-to-noise ratio. The chemical shifts were referenced to adamantane with the upfield methine peak at 29.5 ppm.

2.3. Geometry optimizations

The proton was added to the OSDA manually and further optimized by using the DMol3 program with the generalized gradient approximation (GGA) proposed by Perdew, Burke, and Ernzerhof (PBE). The fine plane wave cutoff energy and a default medium level Monkhorst-Pack K-point in the DMol3 program were adopted to sample the Brillouin zone.

2.4. Rietveld refinement

For the purpose of structural refinement, PXRD data was collected on a PANalytical X'Pert PRO X-ray diffractometer with CuKα radiation (λ = 1.5418 Å) in Bragg-Brentano HD geometry. The 2θ range is 5–90° with a step size of 0.013° and an exposure time of 159.4s. Rietveld refinement is carried out using TOPAS software.

The space group of **CHA** framework is *R*-3*m* (No. 166) and there are one T atom and four O atoms in the asymmetric unit. However, since the distribution of Al and P is alternating in SAPO materials, the space group of type materials such as SAPO-34/44 is reduced to *R*-3 (No. 148). In this case, it means there are two independent crystallographic T sites in the asymmetric unit. Thus, coordinates of Al, P, and O in the **CHA**-type SAPO materials were deduced from the idealized **CHA** framework deposited in the International Zeolite Association (IZA) - Structure Database [34].

Considering a portion of the OSDA in SAPO-34/44 was protonated, the H^{+} of protonated OSDA were evenly distributed to all OSDAs. They were then placed into the unit cell as rigid bodies for locating their positions through the simulated annealing algorithm. For the SAPO-34-DPA, since the propyl group of DPA is flexible, two dihedral angles of DPA were refined in the process of simulated annealing.

3. Result and discussion

The gel compositions of the four samples are listed in Table 1. The PXRD patterns confirm the crystalline phases are pure SAPO-34/44 with a **CHA** FTC, as shown in Fig. S1. The SEM images illustrated in Fig. 1 further confirm the absence of impurity phases, and all the four samples crystallize in rhombohedral morphologies. The size of SAPO-44-CA and SAPO-34-DIPA crystals is ca. 2 μm, while SAPO-34-BA is a little smaller in size, ca. 1.5 μm. Although the larger crystal size of SAPO-34-DPA (ca. 10 μm) can be observed compared with the other three samples, it is still challenging to pick up one single crystal for collecting SCXRD data due to the small crystal size for the in-house SCXRD and the severe twins. The results of solid state ^{13}C NMR have shown that OSDAs remain intact in the as-made SAPO samples as illustrated in Fig. S2.

Chemical compositions of the framework as well as the number of guest water molecules and OSDAs per unit cell are deduced from XRF

Table 1
Gel compositions of the four samples.

Sample	Gel composition[a]
SAPO-44-CA	$2CA:0.8SiO_2:0.8P_2O_5:1Al_2O_3:50H_2O$
SAPO-34-BA	$2BA:1.2SiO_2:0.8P_2O_5:1Al_2O_3:50H_2O$
SAPO-34-DIPA	$3DIPA:0.4SiO_2:1P_2O_5:1Al_2O_3:50H_2O$
SAPO-34-DPA	$3DPA:0.4SiO_2:0.8P_2O_5:1Al_2O_3:100H_2O$

[a] Silicon sources for SAPO-34-BA is fumed silica and others are TEOS. Aluminum source for SAPO-34-DPA is aluminum isopropoxide and the rest is pseudo-boehmite.

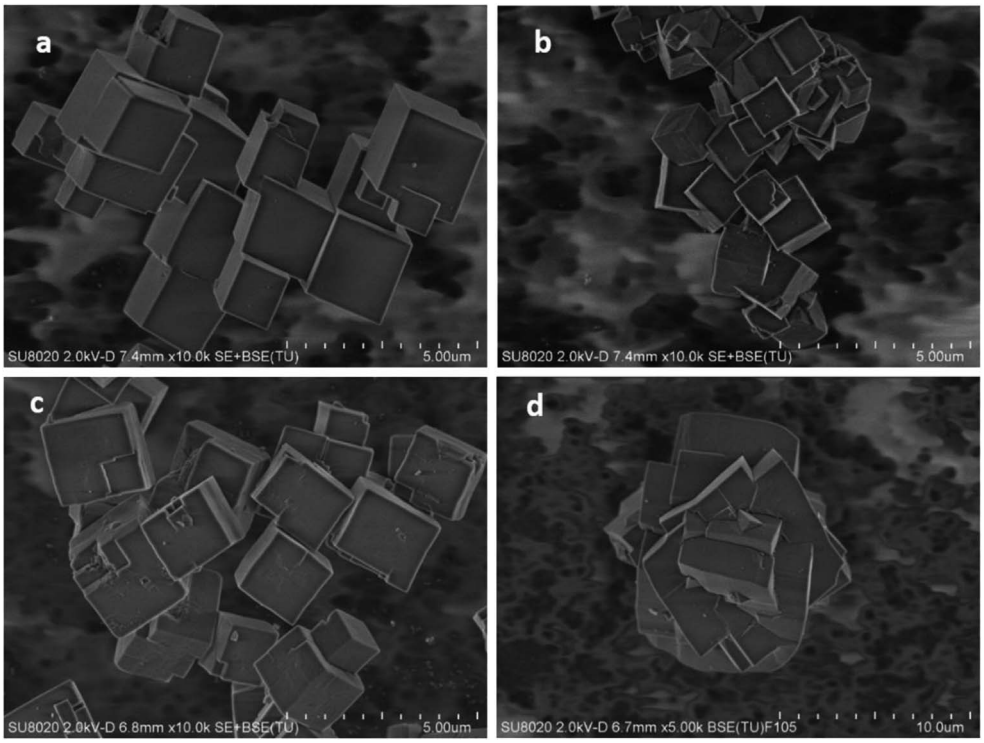

Fig. 1. SEM images of the as-made samples: (a) SAPO-44-CA, (b) SAPO-34-BA, (c) SAPO-34-DIPA, (d) SAPO-34-DPA.

Table 2
Unit cell compositions of the four as-made samples.

Sample	Unit cell composition	Average No. of OSDA per *cha* cage
SAPO-44-CA	$\|CA_{5.7}H_2O_{2.2}H_{3.3}\|[Al_{16.3}Si_{6.7}P_{13.0}O_{72}]$	1.9
SAPO-34-BA	$\|BA_{5.9}H_2O_{2.0}H_{5.5}\|[Al_{15.5}Si_{10.5}P_{10.0}O_{72}]$	2.0
SAPO-34-DIPA	$\|DIPA_{3.1}H_2O_{3.1}H_{2.7}\|[Al_{17.5}Si_{3.7}P_{14.8}O_{72}]$	1.0
SAPO-34-DPA	$\|DPA_{3.2}H_2O_{5.5}H_{2.9}\|[Al_{17.6}Si_{3.7}P_{14.7}O_{72}]$	1.1

and TG results, respectively, as shown in Table 2. Since there are 3 *cha* cages within one unit cell, the number of OSDA per *cha* cage can also be estimated. For the primary cyclamine CA and primary amine BA, each *cha* cage contains approximately two OSDAs. Due to the larger space volume of secondary amine DIPA and DPA, there can be only one OSDA in the *cha* cage. Fig. S3 shows the Raman spectra in the 200-3600 cm^{-1} region of the four as-made sample. One broad band around 3200-3300 cm^{-1} is observed which assignable to N-H stretching mode of neutral amines [35–37]. Therefore, the OSDAs trapped in the *cha* cage are partially protonated. These results are consistent with the analysis results of unit cell chemical compositions deduced from XRF and TG measurements. The presence of NH_2^+/NH_3^+ is further verified by FT-IR spectroscopy shown in Fig. S4. The adsorption ranges 3200 to 3300 cm^{-1} and 1500 to 1600 cm^{-1} are assigned as NH_2^+/NH_3^+ stretching vibration and bending vibration, respectively [29,30]. Unfortunately, TG and IR spectrum results can't provide accurate crystallographic structural information. Thus, the position of the OSDAs and the host-guest interaction between OSDA and inorganic framework are further investigated using a combination of simulated annealing and Rietveld refinement against PXRD data.

Simulated annealing algorithm [38,39], regarded as a direct (real)-space method for structure determination, has been implemented in a large number of crystallographic program suites. Some a priori information such as chemical composition, geometry, and/or connectivity in direct space is required before running simulated annealing. Satisfactory structural models emerge when the difference between the experimental PXRD data and simulated data converges to a global minimum by modifying the positions, orientations and free torsion angles of fragments globally. It has been successfully applied on the structure determination of a 1D 12-ring ALPO molecular sieve Uio-6 (FTC: **OSI**) [40] and a 1D 8-ring aluminosilicate ERS-7 (**ESV**) [41]. For this specific crystalline porous material of molecular sieves, the structure determination contains two parts: 1) determining the framework structure (host) and 2) identifying the inorganic and/or organic SDAs in the channels or cavities (guest species). Since the framework of SAPO-34/44 is known, there is no need to determine. Therefore, in this article, the simulated annealing algorithm is utilized for retrieving the OSDAs from PXRD data accurately.

Among the four samples used in this work, SAPO-44-CA is selected as an example and explained in detail. The blue and red curves as demonstrated in Fig. 2a are experimental PXRD data of as-made SAPO-44-CA and simulated PXRD data of the SAPO **CHA** framework (without CA in the framework), respectively. Since the high angle data isn't affected significantly by guest species in the channel or cavities, the appropriate scale factor between the simulated and experimental data is calculated using data of 40–90° in 2θ. The difference Fourier map (insert in Fig. 2a) is obtained by applying this scale factor to the whole PXRD pattern. It is clear that the electron densities within one *cha* cage are of ring shapes, corresponding to the missing CA OSDAs. Simulated annealing is then employed for locating the positions of the CA OSDAs within the *cha* cage by fixing the framework and considering the OSDAs as rigid bodies. After a few cycles, the position and orientation of the CA OSDAs are determined.

The refinement of SAPO-44-CA (framework and OSDAs) converges to $R_p = 0.069$, $R_{wp} = 0.086$, $R_{bragg} = 0.040$, and GOF = 1.348 (Table S1 and Fig. 2b). The final Rietveld refinement reveals that there are two CA OSDAs in each *cha* cage, which is consistent with the result from TGA. They are in the ***ab***-plane of each *cha* cage with an up-and-down configuration (Fig. 3a). The center of CA OSDA is located on the three-fold axis along the ***c***-axis, generating three equivalent positions. Therefore, the occupancy of each CA OSDA is considered to be 1/3. The

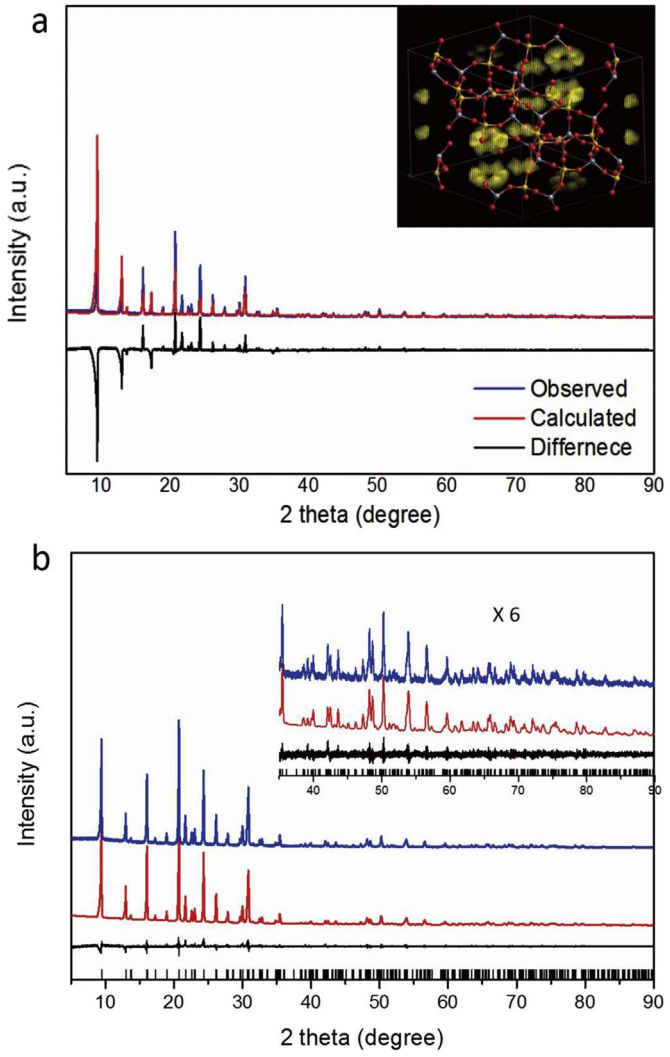

Fig. 2. (a) Plots for finding the OSDA by applying the appropriate scale factor to the whole pattern. The inset is difference electron density map to locate positions of SDAs through Rietveld refinement. (b) Final Rietveld refinement plots of SAPO-44-CA. The observed, calculated, and difference curves are in blue, red, and black, respectively. The vertical bars indicate the positions of Bragg peaks (λ = 1.5418 Å). The inset is the high angle part of the profiles scaled up by a factor of 6. (For interpretation of the references to colour in this figure legend, the reader is referred to the Web version of this article.)

NH_2/NH_3^+ group of CA points towards the 8-ring pore opening. In order to further confirm whether there is an interaction between CA and the framework, the distance between the NH_2/NH_3^+ group of CA and the corresponding O atom of 8-membered ring has been analyzed. The shortest distance, namely N1-H13···O4, is 3.036 Å, showing the classical hydrogen-bonding distance. We note that the location of CA in SAPO-44 has also been refined against SXRD data by Pastore et al. [30], concluding the shortest N···O distance to be 3.293 Å which is comparable with our results.

In the SAPO-34-BA case, the difference Fourier map demonstrates that the residual electron density is also arranged in an up-and-down fashion in the *cha* cage, which is similar to SAPO-44-CA sample. It is challenging to distinguish C and N atoms in the backbone of BA, thus, the amino group is treated to have an even distribution at both ends. The precise locations of BA OSDAs are determined using simulated annealing algorithm as well. The final refinement converged at $R_p = 0.056$ and $R_{wp} = 0.073$ (Table S1 and Fig. S5A). It shows that two BAs lie on the ***ab***-plane in an up-and-down configuration in each *cha* cage (Fig. 3b), matching the TGA results. The NH_2/NH_3^+ group of BA is pointing towards the 8-ring pore opening. Since the three-fold axis along the ***c***-axis is applied to the BA, the occupancy for each BA within one *cha* cage is 1/3 as well. The interaction between BAs and the SAPO framework can be observed through identifying the hydrogen bonding of N1-H7···O2 (3.155 Å). As mentioned before, Pastore et al. also refined a **CHA**-type SAPO form CAL-1 against SCXRD data and found that there were two OSDAs in one *cha* cage. The hydrogen bonding between BA and the framework (N···O distance 3.28 Å-3.59 Å) was also observed in their work [29]. Furthermore, they also investigated the host-guest interaction in a layered aluminophosphate ALPO-ntu framework synthesized by BA. It was found that the N···O distances (2.62–2.82 Å) in the ALPO-ntu structure are much shorter than the one in CAL-1 (3.28 Å-3.59 Å) and our SAPO-34-BA. It indicates that the hydrogen bonding interaction in ALPO-ntu is much stronger than that in SAPO-34-BA. According to the hydrogen-bond theory, the stronger interaction leads to higher wavenumber values of bending vibration and lower values of stretching vibration in the FT-IR spectrum [29,30]. According to the FT-IR spectra of SAPO-34-BA shown in Fig. S4B, the NH_3^+ bending vibration is found at 1620 and 1512 cm^{-1} which are lower than that of ALPO-ntu (1634 and 1555 cm^{-1}), meanwhile the NH_3^+ stretching vibration found at 3290 and 3240 cm^{-1} are higher than that of ALPO-ntu (3120 and 3075 cm^{-1}). Therefore, we conclude that the IR result is consistent with the final Rietveld refinement.

For SAPO-34-DIPA, the difference Fourier map showed a cloud-shaped electron density in the *cha* cage, indicating the distribution of the OSDA may be disordered. The locations and orientations of DIPA are also determined by simulated annealing. The refinement converged to $R_p = 0.085$ and $R_{wp} = 0.114$ (Table S1 and Fig. S5B). It reveals that there is only one DIPA highly disordered distributing in one *cha* cage with a longitudinal arrangement (Fig. 3c). Moreover, the longer distance (3.961 Å) between the NH/NH_{2DIPA}^+ and the $O_{framework}$ in the SAPO-34-DIPA suggests a weak interaction between DIPA and the framework.

The locations of the OSDAs in the SAPO-34-DPA sample are determined by the same approach. Besides, due to the long and flexibility alkyl chain of DPA, two dihedral angles of DPA OSDA were refined. The converged refinement resulted in $R_p = 0.052$ and $R_{wp} = 0.070$ (Table S1 and Fig. S5C). It is interesting to note that the configuration of DPA molecular is bent to be accommodated within the relatively short *cha* cage (Fig. 3d). And the N1-H16···O3 distance is approximately 3.862 Å, which indicates there are only weak interactions between DPA and the SAPO framework. A similar configuration of DPA in *cha* cage of SAPO-34 was obtained through computer simulation reported by Hong and co-workers [37].

4. Conclusions

In this work, the locations and orientations of four individual OSDAs in the *cha* cage of SAPO-34/44 frameworks have been determined through Rietveld refinement and simulated annealing against PXRD data. The interaction (hydrogen bond in the case of SAPO-44-CA and SAPO-34-BA) between the OSDAs and the inorganic frameworks has been analyzed according to the refinement results and corresponding FT-IR spectra. The obtained results may provide insights to the understanding of the crystallization mechanism of SAPO frameworks. Furthermore, it is demonstrated that Rietveld refinement and simulated annealing again PXRD data can be used as a general method for locating guest inorganic and organic species in the channel or cavity of crystalline porous materials. Furthermore, this method can be extended to locate probe molecules in the solid acid SAPO catalysts, providing far-reaching implications regarding the distribution of the acid sites in the framework and their catalytic activities.

Acknowledgement

We acknowledge financial support from National Natural Science Foundation of China (No. 21676262), Key Research Program of

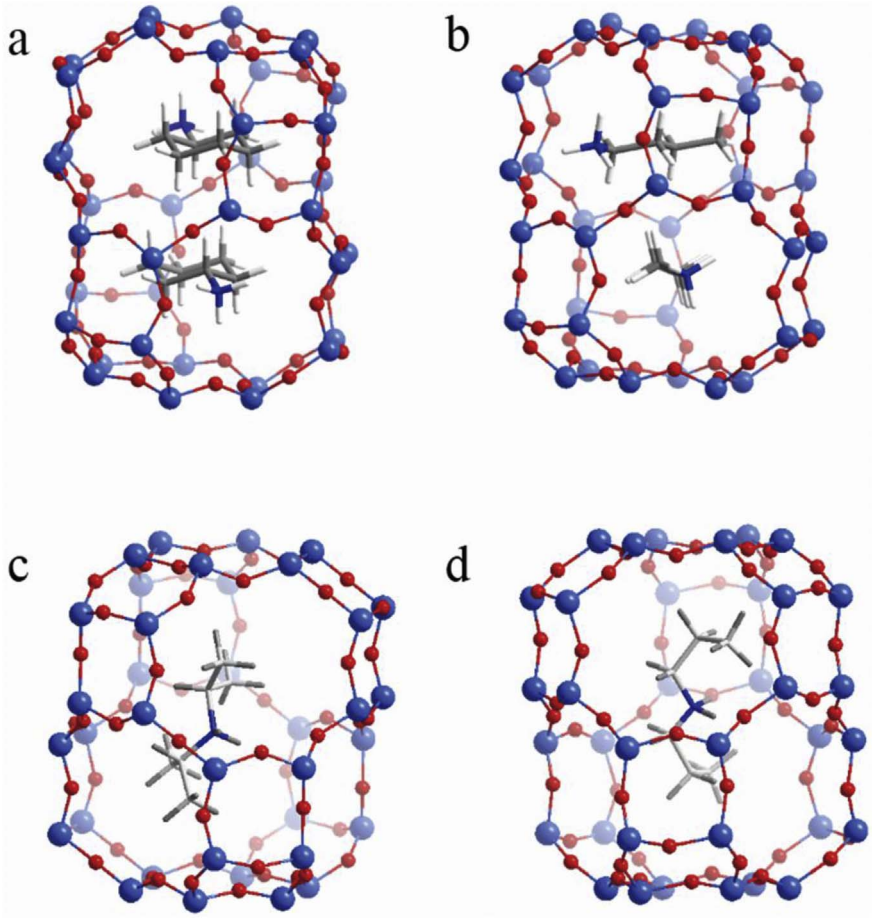

Fig. 3. The locations of OSDAs in the as-made SAPO-34/44 determined by Rietveld refinement and simulated annealing against in-house PXRD data: (a) CA in SAPO-44-CA, (b) BA in SAPO-34-BA, (c) DIPA in SAPO-34-DIPA and (d) DPA in SAPO-34-DPA.

Frontier Sciences, Chinese Academy of Sciences (Grant No. QYZDB-SSW-JSC040), and CAS Pioneer Hundred Talents Program (Y706071202). We would like to thank the anonymous reviewer's insightful suggestion involving the identification of partially protonated OSDAs through the Raman spectrum. We are also grateful to Dr. Jingfeng Han in DICP for his kind help of Raman spectrum measurements.

Appendix A. Supplementary data

Supplementary data related to this article can be found at http://dx.doi.org/10.1016/j.micromeso.2018.01.002.

References

[1] S.T. Wilson, B.M. Lok, C.A. Messina, T.R. Cannan, E.M. Flanigen, J. Am. Chem. Soc. 104 (1982) 1146–1147.
[2] B.M. Lok, C.A. Messina, R.L. Patton, R.T. Gajek, T.R. Cannan, E.M. Flanigen, J. Am. Chem. Soc. 106 (1984) 6092–6093.
[3] M. Hartmann, L. Kevan, Chem. Rev. 99 (1999) 635–664.
[4] Y. Wei, D. Zhang, L. Xu, F. Chang, Y. He, S. Meng, B. Su, Z. Liu, Catal. Today 131 (2008) 262–269.
[5] M. Stöcker, Microporous Mesoporous Mater. 29 (1999) 3–48.
[6] P. Tian, Y. Wei, M. Ye, Z. Liu, ACS Catal. 5 (2015) 1922–1938.
[7] X. Xiang, M. Yang, B. Gao, Y. Qiao, P. Tian, S. Xu, Z. Liu, RSC Adv. 6 (2016) 12544–12552.
[8] T. Yu, D. Fan, T. Hao, J. Wang, M. Shen, W. Li, Chem. Eng. J. 243 (2014) 159–168.
[9] S. Li, J.L. Falconer, R.D. Noble, J. Membr. Sci. 241 (2004) 121–135.
[10] S. Li, J.L. Falconer, R.D. Noble, Adv. Mater. 18 (2006) 2601–2603.
[11] L. Marchese, A. Frache, E. Gianotti, G. Martra, M. Causà, S. Coluccia, Microporous Mesoporous Mater. 30 (1999) 145–153.
[12] P. Sadeghpour, M. Haghighi, Particuology 19 (2015) 69–81.
[13] Y. Qiao, P. Wu, X. Xiang, M. Yang, Q. Wang, P. Tian, Z. Liu, Chin. J. Catal. 38 (2017) 574–582.
[14] D. Fan, P. Tian, S. Xu, D. Wang, Y. Yang, J. Li, Q. Wang, M. Yang, Z. Liu, New J. Chem. 40 (2016) 4236–4244.
[15] E. Dumitriu, A. Azzouz, V. Hulea, D. Lutic, H. Kessler, Microporous Mater. 10 (1997) 1–12.
[16] G. Liu, P. Tian, J. Li, D. Zhang, F. Zhou, Z. Liu, Microporous Mesoporous Mater. 111 (2008) 143–149.
[17] S. Aghamohammadi, M. Haghighi, Adv. Powder Technol. 27 (2016) 1738–1749.
[18] T. Álvaro-Muñoz, C. Márquez-Álvarez, E. Sastre, Catal. Today 179 (2012) 27–34.
[19] J.J. Pluth, J.V. Smith, J. Phys. Chem. 93 (1989) 6516–6520.
[20] G. Nardin, L. Randaccio, V. Kaucic, N. Rajic, Zeolites 11 (1991) 192–194.
[21] P. Huang, J. Xu, G. Qi, F. Deng, R. Xu, W. Yan, Sci. Rep. 6 (2016) srep22019.
[22] A.B. Pinar, L. Gómez-Hortigüela, L.B. McCusker, J. Pérez-Pariente, Chem. Mater. 25 (2013) 3654–3661.
[23] C. Márquez-Alvarez, A.B. Pinar, R. García, M. Grande-Casas, J. Pérez-Pariente, Top. Catal. 52 (2009) 1281–1291.
[24] A.B. Pinar, C. Márquez-Álvarez, M. Grande-Casas, J. Pérez-Pariente, J. Catal. 263 (2009) 258–265.
[25] J. Li, J. Yu, R. Xu, Microporous Mesoporous Mater. 101 (2007) 406–412.
[26] L. Gómez-Hortigüela, F. Corà, C.R.A. Catlow, J. Pérez-Pariente, Phys. Chem. Chem. Phys. 8 (2006) 486–493.
[27] L. Gómez-Hortigüela, F. Corà, C.R.A. Catlow, J. Pérez-Pariente, J. Am. Chem. Soc. 126 (2004) 12097–12102.
[28] F. Fan, Z. Feng, K. Sun, M. Guo, Q. Guo, Y. Song, W. Li, C. Li, Angew. Chem. Int. Ed. 48 (2009) 8743–8747.
[29] C. Gieck, C. Bisio, L. Marchese, Y. Filinchuk, C.E. da Silva, H.O. Pastore, Angew. Chem. Int. Ed. 46 (2007) 8895–8897.
[30] G.A.V. Martins, C. Gieck, S. Coluccia, L. Marchese, H.O. Pastore, J. Phys. Chem. C 113 (2009) 10675–10680.
[31] J.M. Bennett, B.K. Marcus, Stud. Surf. Sci. Catal. 37 (1988) 269–279.
[32] V. Ramaswamy, L.B. McCusker, C. Baerlocher, Microporous Mesoporous Mater. 31 (1999) 1–8.
[33] A. Turrina, R. Garcia, P.A. Cox, J.L. Casci, P.A. Wright, Chem. Mater. 28 (2016) 4998–5012.
[34] International Zeolite Association, Structure Commission, http://www.ica-structure.org.
[35] D. Lin-Vien, N.B. Colthup, W.G. Fateley, J.G. Grasselli, The Handbook of Infrared and Raman Characteristic Frequencies of Organic Molecules, (1974) New York.
[36] Spectral Database for Organic Compounds, http://sdbs.db.aist.go.jp.
[37] B. Han, C.-H. Shin, P.A. Cox, S.B. Hong, J. Phys. Chem. B 110 (2006) 8188–8193.
[38] S. Smeets, L.B. McCusker, C. Baerlocher, S. Elomari, D. Xie, S.I. Zones, J. Am. Chem. Soc. 138 (2016) 7099–7106.
[39] W.I.F. David, K. Shankland, Acta Crystallogr. A 64 (2008) 52–64.
[40] D.E. Akporiaye, H. Fjellvag, E.N. Halvorsen, T. Haug, A. Karlsson, K.P. Lillerud, Chem. Commun. 0 (1996) 1553–1554.
[41] B.J. Campbell, A.K. Cheetham, G. Bellussi, L. Carluccio, G. Perego, R. Millini, D.E. Cox, Chem. Commun. 0 (1998) 1725–1726.